Low-energy structure in the ionization of argon: Comparison of experiment with theory*

Feng Li-Qiang(冯立强)[a], Chu Tian-Shu (楚天舒)[a)b)†], and Wang Li(王 利)[a)‡]

[a] State Key Laboratory of Molecular Reaction Dynamics, Dalian Institute of Chemical Physics, Chinese Academy of Sciences, Dalian 116023, China
[b] Institute for Computational Sciences and Engineering, Laboratory of New Fiber Materials and Modern Textiles, the Growing Base for State Key Laboratory, Qingdao University, Qingdao 266071, China

(Received 4 July 2012; revised manuscript received 3 August 2012)

The above-threshold ionization of argon in an intense 70-fs, 400-nm linearly polarized laser pulse has been investigated by the velocity map imaging techniques, combined with an attosecond-resolution quantum wave packet dynamics method. There is a quantitative agreement in all dominant features between the experiment and the theory. Moreover, a peak-splitting phenomenon in the first energy peak has been observed at high pulse intensity. Further, through the theoretical analysis, an ac Stark splitting with evident resonant and nonresonant ionization pathways has been found to be the physical reason for the experimental observations.

Keywords: above threshold ionization, angular distribution, Stark splitting

PACS: 33.80.Rv, 33.60.+q **DOI:** 10.1088/1674-1056/22/2/023302

1. Introduction

Understanding the motion of the electrons in strong laser fields is a fascinating issue with important implications for making new advances in attosecond physics.[1–4] When atoms are exposed to an intense laser field, the motion of the electrons can be mapped into two regimes, depending on the laser intensity and the wavelength, by using the Keldysh parameter,[5] $\gamma = \sqrt{I_p/(2U_p)}$, where I_p is the ionization potential of the target atom and U_p is the ponderomotive energy of the electron ($U_p = e^2E^2_{laser}/4m_e\omega^2$). Particularly, if $\gamma < 1$, the tunneling ionization becomes dominant.[6,7] In this regime, the mechanism of the emitted electron is dominated by direct ionization. On the other hand, if $\gamma > 1$, in the multiphoton regime, the liberation of the electron is understood to proceed through the absorption of many photons, leading to the above-threshold ionization (ATI)[8] process. The typical features of the photoelectron spectra of ATI are the plateaus in the high-energy part of the spectra[9] and the jet structures accompanied by the sub-peaks in the low-energy part of the spectra.[10] It is widely believed that the high-energy electron is related to the rescattering (recollision) mechanism,[11] while the low-energy part is believed to originate in direct photo-ionization. To date, little research[12–15] has been reported on the intensity dependence of the low-energy structure (LES), especially for a detailed comparison of the current state-of-the-art theory and the experimental data.

Thus, in this paper, we carried out a combined study of ionizing argon with linearly polarized laser pulses (70 fs/400 nm, $I = 0.6\times10^{14}$ W/cm^2–3.2×10^{14} W/cm^2) aiming to explore the features of the electron motion in the ionization process, especially for its role in the formation of the LES (less than 10 eV) in the photoelectron spectrum.

2. Experimental setup

The experimental details of our laser system have been described elsewhere.[16] Briefly, our femtosecond laser is an in-house built, solid-state, chirped-pulse amplified Ti:sapphire femtosecond laser comprising a seed oscillator, an amplifier with a stretcher and a compressor. The fundamental light is centered at 800 nm (with a 30-nm bandwidth, 70-fs pulse width, and 20-Hz repetition rate). The fundamental light is frequency doubled by a β-BaB_2O_4 crystal (BBO, type I) to produce the second harmonic generation (SHG) light, centered at 400 nm. The SHG light is focused by an $f = 30$ cm fused quartz lens and passed into the chamber of a Wiley–McLaren time-of-flight mass spectrometer. Peak intensities at the focus spot could be changed by a neutral density attenuator and are estimated to be from 0.3×10^{14} W/cm^2 to 3.4×10^{14} W/cm^2 at 400 nm.

3. Computational aspects

Our theoretical calculations are carried out by solving the three-dimensional (3D) time-dependent Schrödinger equation (TDSE) based on the single-active electron (SAE) approximation.[17–28] In the dipole approximation and the length gauge, the TDSE is given by (atomic units are used

*Project supported by the National Natural Science Foundations of China (Grant Nos. 10874096 and 20633070).
†Corresponding author. E-mail: tschu@dicp.ac.cn; tschu008@163.com
‡Corresponding author. E-mail: liwangye@dicp.ac.cn
© 2013 Chinese Physical Society and IOP Publishing Ltd

throughout this paper unless stated otherwise)

$$\mathrm{i}\frac{\partial\phi(r,t)}{\partial t}=\left[-\frac{1}{2}\nabla^2+V(r)+rE(t)\right]\phi(r,t). \quad (1)$$

The time-dependent wave function $\phi(r,t)$ can be expanded as

$$\phi(r,t)=\sum_{l=0}^{l_{\max}=48}\sum_{m=-l}^{m=l}\frac{1}{r}\chi_l(r,t)\mathrm{Y}_l^m(\theta,\varphi), \quad (2)$$

where $\chi_l(r,t)$ and $\mathrm{Y}_l^m(\theta,\varphi)$ are the radial and the spherical harmonic functions. Because a linearly polarized field is used, only a spherical harmonic with $m=0$ has been introduced for simplicity. With the wave function in this expression the TDSE can be solved by a set of coupled partial differential equations

$$\begin{aligned}\mathrm{i}\frac{\partial}{\partial t}\chi_l(r,t) &= \left[-\frac{1}{2}\frac{\partial^2}{\partial r^2}+V(r)+\frac{l(l+1)}{2r^2}\right]\chi_l(r,t)\\ &\quad +rE(t)[c_l^+\chi_{l+1}(r,t)+c_l^-\chi_{l-1}(r,t)], \quad (3)\end{aligned}$$

where $c_l^{\pm}$ are the coupling constants related to Clebsch–Gordan coefficients, having the form

$$c_l^+=c_{l+1}^-=\sqrt{\frac{(l+1)^2}{(2l+3)(2l+1)}}, \quad (4)$$

and the initial wave function is chosen to be $\chi_{\mathrm{initial}}(r,t)=\chi_1(r,t)$ (3p state with $l=1$).

$$V(r)=-\frac{Z+a_1\,\mathrm{e}^{-a_2r}+a_3r\,\mathrm{e}^{-a_4r}+a_5\,\mathrm{e}^{-a_6r}}{r}$$

is the effective atomic potential with $Z=1.0$, $a_1=16.039$, $a_2=2.007$, $a_3=-25.534$, $a_4=4.525$, $a_5=0.961$, $a_6=0.443$ to match the ionization potential of 15.76 eV for the ground state of a real argon atom.[29] The linearly polarized laser field is expressed as $E(t)=E\sin^2(\pi t/T)\cos(\omega t)$. Further, in the propagated process, the time-dependent wave function can be advanced using the standard second-order split-operator method:[30,31]

$$\chi_l(t+\delta t)=\mathrm{e}^{-\mathrm{i}K_T\delta t/2}\,\mathrm{e}^{-\mathrm{i}V\delta t}\,\mathrm{e}^{-\mathrm{i}K_T\delta t/2}\chi_l(t)+O(\delta t^3), \quad (5)$$

where K_{T} and V are the kinetic-energy operator and the interaction potential, respectively.

The angular distributions and the photoelectron energy spectra can be extracted by projecting the final wave function at the end of the pulse onto the continuum field-free wave functions:[32]

$$\begin{aligned}P(\theta) &= \left|\sum_{l=0}^{l_{\max}}i^l\exp\left(-\mathrm{i}\sum_{l'=1}^{l}\arctan(-1/\sqrt{2El'})\right)\mathrm{Y}_l^0(\theta)\right.\\ &\quad \left.\times\int\chi_l^c(E,r)\chi_l(r,t=T)\,\mathrm{d}r\right|^2, \quad (6)\end{aligned}$$

$$P(E,T)=\sum_{l=0}^{l_{\max}}P_l(E,T), \quad (7)$$

and

$$P_l(E,t=T)=\left|\int_0^{R_{\max}}\chi_l^c(E,r)\chi_l(r,t=T)\,\mathrm{d}r\right|^2, \quad (8)$$

where P_l is the partial angular ATI contribution.

4. Results and discussion

4.1. Comparison between experiment and theory

Figures 1(a) and 1(c) show a selection of two pairs of experimental images ($I=0.8\times10^{14}$ W/cm^2, top row and $I=1.4\times10^{14}$ W/cm^2, bottom row), which we consider representative of the various regimes encountered. Our theoretical simulation is also shown in this figure (Figs. 1(b) and 1(d)). Clearly, we see that the experimental data have been reproduced very well by the theory, and the emitted electrons are predominantly distributed along the polarization direction.

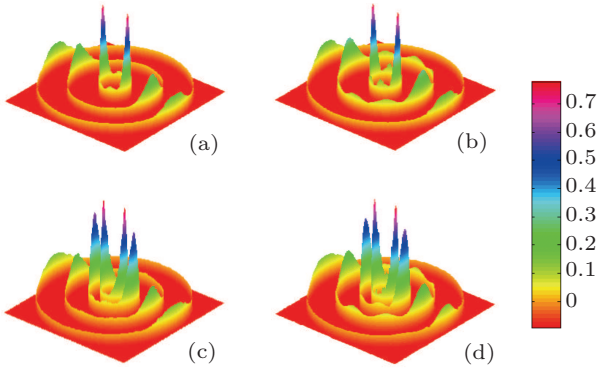


Fig. 1. (color online) 3D angular distributions of the ATI spectra under a 70-fs/400-nm pulse with $I=0.8\times10^{14}$ W/cm^2 [(a) and (b)], and $I=1.4\times10^{14}$ W/cm^2 [(c) and (d)]. Experiment: left column; theory: right column.

For a clear observation of the LES, in Fig. 2, we show the (experimental and theoretical) low-energy ATI spectra (less than 10 eV) and the angular distributions of the emitted electron for each of the ATI peaks. Figures 2(a) and 2(e) show the low-energy ATI spectra for the above two selected pulse intensities. It can be seen that, at the low intensity (Fig. 2(a)), the ATI spectra are well documented showing three main ATI peaks which are regularly separated by the photon energy of 3.1 eV. However, at the high pulse intensity (Fig. 2(e)), both the experiment and the theory demonstrate that the 1st ATI peak is split into two subpeaks with a splitting energy space of 0.42 eV. Figures 2(b)–2(d) and 2(f)–2(i) show the angular distributions of the corresponding ATI peaks for the two pulse intensities. Clearly, except for the dominant emitted direction as seen in Fig. 1, there are some subtle emissions in other directions due to the presence of several small subpeaks. Particularly, there are respectively two, three, and four subpeaks between 0° and 180° for the 1st (sub2 for the high pulse intensity), the 2nd, and the 3rd ATI peaks.

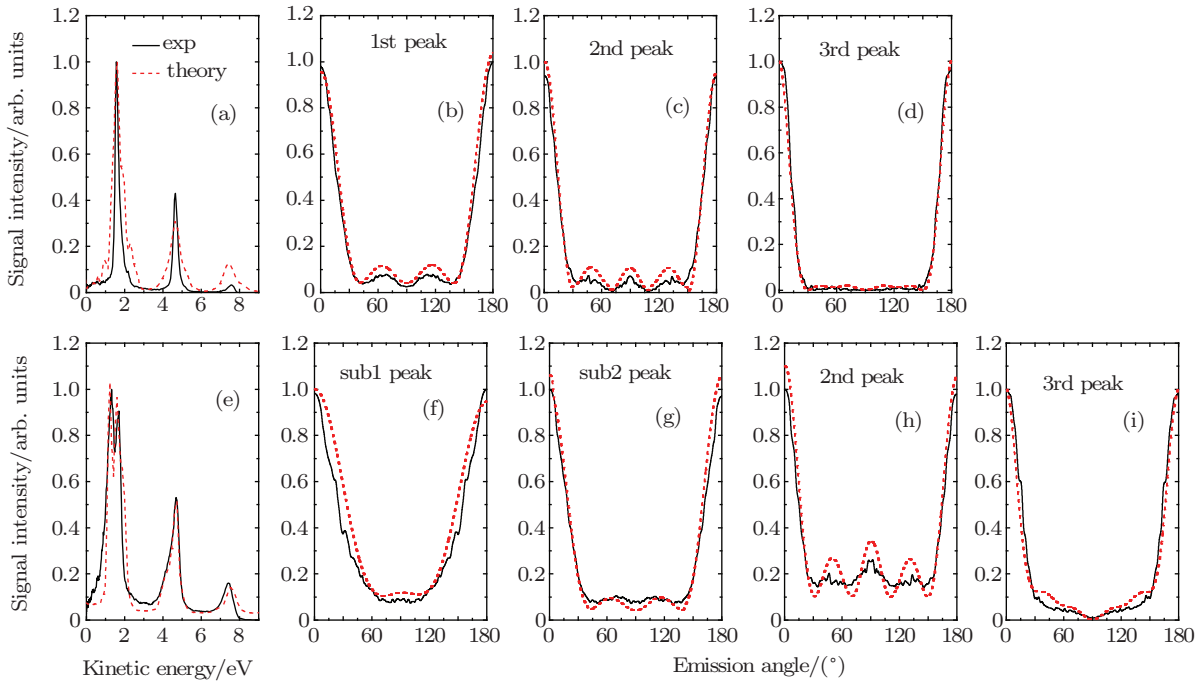


Fig. 2. (color online) ATI spectra and the angular distributions of the first three ATI peaks. Top row, $I = 0.8\times10^{14}$ W/cm^2; bottom row, $I = 1.4\times10^{14}$ W/cm^2. Experiment: solid black line; theory: dashed red line.

4.2. Theoretical analysis

4.2.1. *l*-states contributions and angular distributions

As of now, the agreement between the experiment and the theory is fully established. Then, to better understand the physical origin of the LES, a detailed analysis to explore the electron motion is necessary.

By carrying out the 3D-TDSE calculations and using Eq. (8), we obtain the l-states? contributions of the above two ATI spectra, as shown in Table 1. Clearly, we see that the 1st (sub2 at high pulse intensity), the 2nd, and the 3rd ATI peaks receive dominant contributions from the angular states with $l = 3$, $l = 4$, and l=5, respectively. Further, through analyzing the spherical harmonics functions, we see that the $l = 0$ state (s state) is spherical symmetry and the $l > 0$ states will have $l - 1$ subpeaks between 0° and 180°. Therefore, the respective number of the subpeaks in the angular distributions for each of the ATI peaks (i.e., 2, 3, 4 at low intensity), as mentioned above, is just the rough reflection of the main l-states? contributions received by these ATI peaks. It is noted that for the high pulse intensity, the 3rd peak receives two similar contributions from $l = 3$ and 5 states. However, it causes no obvious changes on the subpeaks between 0° and 180° (still four subpeaks but with different positions).

Table 1. Angular momentum states? (l-states) contributions to each ATI peak.

Pulse intensity	Peak		$l = 0$(%)	$l = 1$(%)	$l = 2$(%)	$l = 3$(%)	$l = 4$(%)	$l = 5$(%)	$l = 6$(%)	$l = 7$(%)
0.8×10^{14} W·cm^{-2}	1st			12		61		8		9
	2nd		3		26		42		20	
	3rd			3		25		48		15
1.4×10^{14} W·cm^{-2}	1st	Sub1		52		39		5		
		Sub2		18		53		13		11
	2nd		2		30		47		18	
	3rd			7		39		34		18

4.2.2. Resonant/nonresonant ionization and Stark splitting

As can be seen, the most important characteristic of the ATI spectra is the 1st-peak-splitting. Therefore, to further understand this peak-splitting, in Fig. 3, we present the total ATI spectra as a function of the pulse intensities. Clearly, according to the position of the peaks, we see that the sub2 peak is a resonant ionization process (where the peaks always appear at the same electron energy at any intensity). Moreover,

based on the dipole selection rules, the electron must be in either the $l = 2$ or the $l = 4$ state prior to ionization in order to populate the $l = 3$ state (the dominant state to the sub 2 peak as seen from Table 1). Further, through analyzing the energy levels,[33] we can confirm that the sub2 peak is safely attributable to resonant ionization through the 3d state. However, the sub1 peak, unlike the sub2 peak with Freeman resonances, shifts toward the low-energy part as the pulse intensity increases, thus revealing a nonresonant ionization process. Based on the dipole selection rules, the electron should be in the $l = 0$ or $l = 2$ state prior to ionization in order to populate states with $l = 1$ (the dominant contribution to sub1), and through analyzing the energy levels,[33] we know that the sub1 peak is attributable to the 5s state ionization. Actually the energies of the 3d and the 5s states are very close (the energy difference is approximately 0.41 eV),[33] thus, they are almost resonantly coupled at low pulse intensity, which is responsible for the single ATI peak observed. However, as the pulse intensity is enhanced, the electron has to overcome a certain ponderomotive energy (proportional to U_p) attributable to its oscillatory motion in the laser field, and more energy needs to be deposited in the system for ionization. Thus, the coupling will repel these two states and further cause the Stark splitting of the 1st ATI peak.[14] In addition, by calculating the ATI spectra at different frequencies (360 nm–420 nm, which are not shown in this paper), we find that this first-peak-splitting is a universal phenomenon at high pulse intensity (at least for the multiphoton regime).

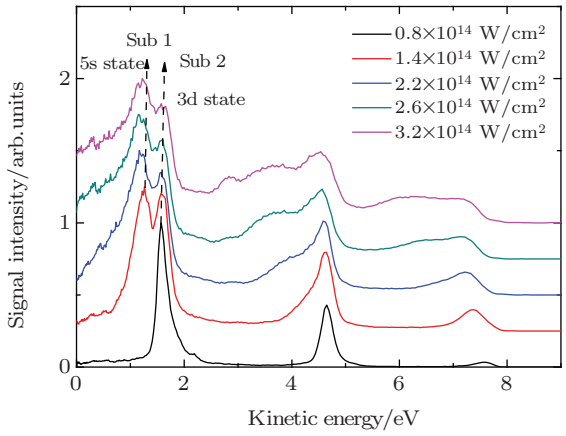


Fig. 3. (color online) The ATI spectra as a function of pulse intensity. Black line: $I = 0.8 \times 10^{14}$ W/cm^2; red line: $I = 1.4 \times 10^{14}$ W/cm^2; blue line: $I = 2.2 \times 10^{14}$ W/cm^2; dark cyan line: $I = 2.6 \times 10^{14}$ W/cm^2; magenta line: $I = 3.2 \times 10^{14}$ W/cm^2.

5. Conclusion

In conclusion, both the velocity mapping experiment and the 3D-TDSE analysis have been employed to investigate the electron motion in argon atoms ionizing with 70-fs/400-nm linearly polarized laser pulses. Agreement between experiment and theory is quite good for the total ATI spectra and the angular distributions at each ATI peak. A peak-splitting phenomenon in the first ATI peak has been observed at high pulse intensity. Further, based on the TDSE analysis, the origin of this peak-splitting on the LES is linked to the Stark splitting of the 5s/3d coupled Rydberg states, and it is revealed that the sub1 peak is caused by the nonresonant ionization pathway while the sub2 peak is formed by the resonant ionization pathway.

References

[1] Kothari H N and Joshipura K N 2010 *Chin. Phys.* B **19** 103402
[2] Chang P S, Song F Z, Jian H C and Xiao X Z 2011 *Chin. Phys.* B **20** 113201
[3] Wang D H 2011 *Chin. Phys.* B **20** 013403
[4] Wu J H and Yuan J M 2009 *Chin. Phys.* B **18** 5283
[5] Keldysh L V 1965 *Sov. Phys. JETP* **20** 1307
[6] Chen J 2002 *Phys. Rev.* A **66** 053415
[7] Moshammer R, Ullrich J, Feuerstein B, Fischer D, Dorn A, Schröter C D, Crespo Lopez-Urrutia J R, Hoehr C, Rottke H, Trump C, Wittmann M, Korn G and Sandner W 2003 *Phys. Rev. Lett.* **91** 113002
[8] Agostini P, Fabre F, Mainfray G, Petite G and Rahman N K 1979 *Phys. Rev. Lett.* **42** 1127
[9] Muller H G 1999 *Phys. Rev.* A **60** 1341
[10] Quan W, Lin Z, Wu M, Kang H, Liu H, Liu X, Chen J, Liu J, He X T, Chen S G, Xiong H, Guo L, Xu H, Fu Y, Cheng Y and Xu Z Z 2009 *Phys. Rev. Lett.* **103** 093001
[11] Corkum P B 1993 *Phys. Rev. Lett.* **71** 1994
[12] Morishita T, Chen Z.J, Watanabe S and Lin C D 2007 *Phys. Rev.* A **75** 023407
[13] Nepstad R, Hart H W and McCann J F 2009 *J. Phys.* B: *At. Mol. Opt. Phys.* **42** 145603
[14] Wiehle R, Witzel B, Helm H and Cormier E 2003 *Phys. Rev.* A **67** 063405
[15] Lemell C, Dimitriou K I, Tong X M, Nagele S, Kartashov D V, Burgdörfer J and Gräfe S 2012 *Phys. Rev.* A **85** 011403
[16] Guo W, Zhu J, Wang B, Wang Y and Wang L 2008 *Phys. Rev.* A **77** 033415
[17] Lu R F, Zhang P Y and Han K L 2008 *Phys. Rev.* E **77** 066701
[18] Hu J, Han K L and He G Z 2005 *Phys. Rev. Lett.* **95** 123001
[19] Meng Q T, Yang G H, Sun H L, Han K L and Lou N Q 2003 *Phys. Rev.* A **67** 063202
[20] Muller H G and Kooiman F C 1998 *Phys. Rev. Lett.* **81** 1207
[21] Feng L Q and Chu T S 2011 *Phys. Rev.* A **84** 053853
[22] Lu R F, He H X, Guo Y H and Han K L 2009 *J. Phys.* B: *At. Mol. Opt. Phys.* **42** 225601
[23] He H X, Lu R F, Zhang P Y, Han K L and He G Z 2012 *J. Chem. Phys.* **136** 024311
[24] Hu J, Wang M S, Han K L and He G Z 2006 *Phys. Rev.* A **74** 063417
[25] He H X, Lu R F, Zhang P Y, Guo Y H, Han K L and He G Z 2011 *Phys. Rev.* A **84** 033418
[26] Zhang H, Han K L, Zhao Y, He G Z and Lou N Q 1997 *Chem. Phys. Lett.* **271** 204
[27] Hu J, Meng Q T and Han K L 2007 *Chem. Phys. Lett.* **442** 17
[28] Guo Y H, Lu R F, Han K L and He G Z 2009 *Int. J. Quantum Chem.* **109** 3410
[29] Tong X M and Lin C D 2005 *J. Phys.* B: *At. Mol. Opt. Phys.* **38** 2593
[30] Chu T S, Zhang Y and Han K L 2006 *Int. Rev. Phys. Chem.* **25** 201
[31] Xie T X, Zhang Y, Zhao M Y and Han K L 2003 *Phys. Chem. Chem. Phys.* **5** 2034
[32] Chen X S, Sanpera A and Burnett K 1995 *Phys. Rev.* A **51** 4824
[33] Minnhagen L 1973 *J. Opt. Soc. Am.* **63** 1185